The linear dependence of polar cap index on its controlling factors in solar wind and magnetotail

Ye Gao,[1,2] Margaret G. Kivelson,[1,2,3] and Raymond J. Walker[1,2]

[1] The solar wind is coupled to the magnetosphere-ionosphere system through various interactions, e.g., magnetic reconnection at the dayside magnetopause, and viscous interactions at the low latitude boundary layer. The polar cap, a region of open magnetic flux connecting the magnetic field of the Earth to that of the solar wind, is an ideal region in which to investigate how solar wind drives the magnetosphere-ionosphere dynamo. For such studies, the polar cap (PC) index provides a useful characterization of the state of the polar ionosphere. A previous study by Gao et al. (2012a) found that polar cap dynamics, characterized by the PC index, responds to both solar wind driving quantified by the electric field ($E_{\text{K-R}}$) proposed by Kivelson and Ridley (2008) which is a representative of the electric field imposed on the ionosphere by magnetopause reconnection that takes cross polar cap potential saturation into account, and the energy release in the magnetotail, described by a modified AL index (AL_{U}). In that study, the dependence of the PC index on $E_{\text{K-R}}$ and AL_{U} was investigated assuming a linear relationship. In this study, we test the assumption that the relationship is linear by performing a similar analysis applying a more general, nonlinear model to the events of the Gao et al. (2012a) study. A nonlinear relationship can be established by use of a statistical approach referred to as the additive model. We find that the more flexible additive model outperforms the linear model. However, the improvement is small. Provided that $E_{\text{K-R}}$ is used to characterize the solar wind input, results obtained from the additive model are very similar to those from the linear model. This result indicates that the linear relation between the PC index and $E_{\text{K-R}}$, AL_{U} obtained by Gao et al. (2012a) represents the data within fluctuations.

1. Introduction

[2] The polar cap (PC) index was introduced by *Troshichev et al.* [1988] as an instantaneous measure of polar cap dynamics driven by the interplanetary magnetic field (IMF) and the solar wind. It has been argued that among various solar wind-magnetosphere coupling functions, the polar cap magnetic field fluctuation most closely relates to the merging electric field [*Kan and Lee*, 1979] imposed by reconnection at the dayside magnetopause,

$$E_{\text{K-L}} = u B_{YZ} \sin^2 \theta / 2, \qquad (1)$$

where u is the magnitude of the solar wind velocity, $B_{YZ} = (B_Y^2 + B_Z^2)^{1/2}$ in the GSM coordinate system, and θ is the IMF clock angle measured from the GSM Z axis. Thus, the PC index was calibrated as a monitor of the merging electric field [*Troshichev et al.*, 1988]. (See *Stauning* [2011] for a detailed discussion of the derivation of the PC index used in this study.)

[3] Statistical analyses have demonstrated that the PC index is representative of diverse ionospheric processes. For example, *Troshichev et al.* [1996] related the PC index to the cross polar cap potential (Φ_{PC}) measured by the EXOS-D satellite and obtained a linear relationship,

$$\Phi_{\text{PC}}[\text{kV}] = 19.35\text{PC} + 8.78. \qquad (2)$$

Ridley and Kihn [2004] took seasonal effects into account and proposed a different formula to convert from polar cap index to the cross polar cap potential measured by AMIE,

$$\Phi_{\text{PC}}[\text{kV}] = 29.28 - 3.31\sin(T + 1.49) + 17.81\text{PC}, \qquad (3)$$

where T is the month of the year normalized to 2π (i.e., Jan. = 0, Jul. = $6 \times 2\pi/12$, Dec. = $11 \times 2\pi/12$). *Troshichev et al.* [2000] found that the cross polar electric field

[1]Department of Earth and Space Sciences, UCLA, Los Angeles, California, USA.
[2]Institute of Geophysics and Planetary Physics, UCLA, Los Angeles, California, USA.
[3]Department of Atmospheric, Oceanic and Space Sciences, University of Michigan, Ann Arbor, Michigan, USA.

Corresponding Author: Y. Gao, Department of Earth and Space Sciences, UCLA, 595 Charles Young Dr. E., Los Angeles, CA 90095, USA. (ygao@igpp.ucla.edu)

measured by DMSP is well represented by a second order polynomial of the PC index. *Fiori et al.* [2009] studied the relationship between the plasma convection velocity and the PC index and got similar results. *Liou et al.* [2003] examined the statistical relationship between auroral power and the polar cap index and found a reasonably large correlation coefficient (0.7). *Chun et al.* [1999, 2002] have shown that the PC index can serve as a proxy for the hemispheric Joule heating production rate and claimed that it is possible to predict the Joule heating pattern from the PC index.

[4] Despite the general success in relating polar cap dynamics as quantified by the PC index to solar wind driving and magnetotail activity, few studies have paid attention to times of intense geomagnetic activity. However, the saturation of the cross polar cap potential at such times has been extensively discussed [e.g., *Russell et al.*, 2000; *Nagatsuma*, 2002; *Shepherd et al.*, 2002; *Siscoe et al.*, 2002, 2004; *Kivelson and Ridley*, 2008]. In exploring the physical mechanism of cross polar cap potential saturation, *Kivelson and Ridley* [2008] took into consideration the partial reflection of the merging electric field at the top of the ionosphere and proposed that the observed electric field in the ionosphere would take the form

$$E_{\text{K-R}} = E_{\text{K-L}} \, 2\Sigma_A/(\Sigma_P + \Sigma_A), \tag{4}$$

where $2\Sigma_A/(\Sigma_P + \Sigma_A)$ is the transmission coefficient. In equation (4), Σ_A is the Alfvén conductance of the solar wind calculated as

$$\Sigma_A = 1/\mu_0 v_A, \tag{5}$$

where $v_A = B/(\mu_0\rho_{\text{sw}})^{1/2}$ is the Alfvén velocity in solar wind, ρ_{sw} is the solar wind mass density, $\mu_0 = 4\pi \times 10^{-7}$H/m is the permeability of the free space, and Σ_P is the ionospheric Pedersen conductance, fixed to be 10S in the analysis that follows as suggested by *Kivelson and Ridley* [2008]. For nominal solar wind conditions, $v_A \approx 50$ km/s, and therefore $\Sigma_A = 1/\mu_0 v_A \approx 16$S, which is close to Σ_P. Thus, $E_{\text{K-R}} \approx E_{\text{K-L}}$. Nevertheless, under strong solar wind driving, Σ_A decreases significantly as v_A increases and satisfies $\Sigma_A < \Sigma_P$, and thus, $E_{\text{K-R}} < E_{\text{K-L}}$. Y. Gao et al. (Utilizing the polar cap index to explore strong driving of polar cap dynamics, submitted to *Journal of Geophysical Research*, 2012) performed a similar analysis with $\Sigma_P = 5$S and 15S, and found that the results are consistent with those obtained when $\Sigma_P = 10$S. This is because, in equation (4), Σ_P establishes the threshold below which saturation occurs, i.e., $\Sigma_A < \Sigma_P$. However, for our events, when saturation occurred, the condition $\Sigma_A < \Sigma_P$ was strongly satisfied and the results were insensitive to the exact threshold value. Therefore, the conclusions of our study are not sensitive to limited variations of Σ_P (e.g., 5S $\leq \Sigma_P \leq$ 15S). Theoretical analysis [*Kivelson and Ridley*, 2008], simulation results [*Borovsky et al.*, 2009] and data analysis (Gao et al., submitted manuscript, 2012) all support the idea that $E_{\text{K-R}}$ is a better indicator of the electric field in the ionosphere caused by the dayside reconnection than is $E_{\text{K-L}}$, especially when $E_{\text{K-L}}$ is unusually large (e.g., $E_{\text{K-L}} > 10$ mV/m).

[5] Different mechanisms have been proposed to explain the saturation of the cross polar cap potential under strong solar wind driving. For example, *Siscoe et al.* [2002, 2004], who adopted and developed the model by *Hill et al.* [1976], argued that the saturation of cross polar cap potential results from a feedback in which the magnetic field generated by Region-1 current becomes comparable to and opposes the Earth's dipole field at the magnetopause where reconnection occurs. By significantly weakening the field that is reconnecting, the Region-1 current ultimately limits how fast reconnection occurs, resulting in the saturation of cross polar cap potential. Although the physical mechanism proposed by *Siscoe et al.* [2002, 2004] is fundamentally different from that by *Kivelson and Ridley* [2008], the predicted electric fields from the two models are similar. It is not the purpose of this paper to explore which model is correct and, essentially, all saturation models predict the saturated electric field in forms similar to equation (4) [e.g., *Borovsky et al.*, 2009]. Thus, we employ $E_{\text{K-R}}$ as a representative of the electric field imposed on the polar ionosphere by magnetopause reconnection that takes saturation into account. For other models of cross polar cap potential saturation, see *Borovsky et al.* [2009].

[6] Although solar wind driving contributes substantially to polar cap dynamics, Gao et al. (submitted manuscript, 2012) found that the PC index not only responds to $E_{\text{K-R}}$, i.e., the driven contribution, but also responds to magnetotail activity. The AL index, a similar measure of geomagnetic activity, provides a measure of high latitude nightside currents. In statistical analyses of the index, a significant part of its variability is linked to substorms, and this part is referred to as the unloading contribution [*Akasofu*, 1979; *Bargatze et al.*, 1985; *McPherron and Baker*, 1993; Gao et al., submitted manuscript, 2012]. However, there is also an AL response directly linked to the solar wind electric field. It is, thus, customary to regard AL as a sum of the unloading, or nightside, contribution (here denoted as AL_U) and the directly driven, or dayside contribution (here denoted as AL_D), which implies that

$$\text{AL}_U = \text{AL} - \text{AL}_D. \tag{6}$$

Gao et al. (submitted manuscript, 2012) have calculated AL_D by regressing AL on $E_{\text{K-R}}$, i.e.

$$\text{AL}_D = \alpha_0 + \alpha_1 E_{\text{K-R}}, \tag{7}$$

where α_0 is the intercept, and α_1 is the regression coefficient.

[7] In order to quantify the relative importance between $E_{\text{K-R}}$ and AL_U, standardization procedures are applied to both $E_{\text{K-R}}$ and AL_U, i.e., $zs(E_{\text{K-R}})$ and $zs(\text{AL}_U)$, by calculating the normalized quantities referred to as z-scores, defined as

$$zs(X) = (X - \mu_X)/\sigma_X, \tag{8}$$

where X is a variable with expectation μ_X and standard deviation σ_X. In practice, μ_X is estimated from sample mean $(\bar{x})$, i.e.

$$\mu_X \approx \bar{x} = \sum_i x^{(i)}/n, \tag{9}$$

where $x^{(i)}$ represents the ith observation, and n is the sample size. σ_X is estimated from sample standard deviation (s), i.e.

$$\sigma_X \approx s = \left[\Sigma_i \left(x^{(i)} - \bar{x} \right)^2 / (n-1) \right]^{1/2}. \qquad (10)$$

[8] The relation between PC and $E_{\text{K-R}}$, AL_{U} can be summarized as [*Gao et al.*, 2012; Gao et al., submitted manuscript, 2012]

$$\text{PC} = \beta_0 + \beta_1 zs(E_{\text{K-R}}) + \beta_2 zs(\text{AL}_{\text{U}}) + \varepsilon_{\text{L}}, \qquad (11)$$

where β_0 is the intercept, β_1 and β_2 are regression coefficients and ε_{L} is the Gaussian noise with zero expectation and constant variance, i.e., $\text{E}(\varepsilon_{\text{L}}) = 0$ and $\text{var}(\varepsilon_{\text{L}}) = \text{const}$. With PC related to the normalized proxies of $E_{\text{K-R}}$ and AL_{U}, their relative importance in determining the PC index is given by the relative magnitudes of the regression coefficients β_1 and β_2.

[9] Equation (11) assumes that the PC index is linearly related to $E_{\text{K-R}}$ and AL_{U}. We next investigate whether this assumption is valid by employing a more general, nonlinear model to relate these two quantities to the PC index. Our approach is based on using a nonlinear relation called the additive model, which we describe below. We ask whether a nonlinear form of the relationship among the quantities of interest is substantially more successful in predicting the PC index than the linear model. Our objective is to determine the potential optimum predictor of the effect of solar wind parameters on polar cap dynamics, as represented by the PC index.

[10] In section 2, we describe the data used. In section 3, we apply additive (nonlinear) analysis to the events used by Gao et al. (submitted manuscript, 2012) and compare the results with those obtained by linear regression analysis. We find that (1) the additive model outperforms the linear model in all cases; (2) the improvements by switching from the linear model to the additive model are relatively small, which confirms the validity of the linear assumption; (3) the fitted values of PC index from the additive model are very similar to those obtained from the linear model; (4) the results from both models are adequate. Finally, we summarize the results in section 4 and compare the nonlinear, additive model to the linear model.

2. Data

[11] In this study, one-minute resolution PC index data from the northern hemisphere (PCN) are used because they provide a more continuous data set than the PC index from the southern hemisphere (PCS). The events used in this study are those used in Gao et al. (submitted manuscript, 2012) who selected 53 one or two-day intervals with subintervals during which $E_{\text{K-L}} > 10$ mV/m from 1998 to 2006. The PCN index data come from magnetic data from the Qaanaaq station (86.5° magnetic latitude) and are produced by the Danish National Institute (DTU space); the PCS index is from Vostok ($-83.4°$ magnetic latitude) magnetic data and is produced by the Arctic and Antarctic Research Institute [*Troshichev and Lukianova*, 2002].

[12] The solar wind data are provided by instruments on the ACE spacecraft located at Lagrange point 1 ($L1$). The one-minute magnetic field vector and plasma moments are obtained from the Magnetic Field (MAG) [*Smith et al.*, 1998] and Solar Wind Electron, Proton, and Alpha Monitor (SWEPAM) [*McComas et al.*, 1998] instruments. The GSM coordinate system is adopted for analyzing plasma velocity and magnetic field observations. The solar wind observations have been propagated to $X_{\text{GSM}} = 17 \, R_{\text{E}}$ using the techniques of *Weimer et al.* [2003].

[13] The AE index obtained from the World Data Center in Kyoto comes from the geomagnetic variations in the horizontal component observed at 12 selected observatories near the auroral zone in the northern hemisphere. The data from these stations are superposed as a function of UT. AU and AL form the upper envelope and lower envelope of the superposed traces, respectively. The difference, AU $-$ AL, defines the AE index.

3. Analysis

[14] Our goal is to model the dependence of PCN on a set of potentially important predictors for at least three reasons. The first is to describe the dependence of PCN on the predictors. The second is to access the relative contributions of the predictors in controlling PCN. The third is to predict PCN values to, say, identify unusual activity. Gao et al. (submitted manuscript, 2012) identified two important predictors: the modified electric field ($E_{\text{K-R}}$), taken as a representative of the polar cap electric field imposed by dayside reconnection, a form in which saturation is taken into account; and the modified AL index (AL_{U}). The standard tool used was the multiple linear regression model given in equation (11) and is rewritten below,

$$\text{PCN} = \beta_0 + \beta_1 zs(E_{\text{K-R}}) + \beta_2 zs(\text{AL}_{\text{U}}) + \varepsilon_{\text{L}}, \qquad (12)$$

where β_0 is the intercept, β_1 and β_2 are regression coefficients and ε_{L} is Gaussian noise [*Hastie and Tibshirani*, 1990; *Myers*, 2000]. In equation (12), the solar wind data are propagated to $X_{\text{GSM}} = 17 \, R_{\text{E}}$ by using the technique of *Weimer et al.* [2003]. For each individual event, an extra time shift (ΔT) is added to the solar wind data to achieve the highest cross correlation between $E_{\text{K-R}}$ and the PCN index. Using the data set of Gao et al. (submitted manuscript, 2012), the histogram of ΔT is shown in Figure 1, which can be numerically summarized as: mean: 12.98; standard deviation: 15.90; minimum: -47; 1st quartile: 7.75; median: 12; 3rd quartile: 17.25; maximum: 59. This $E_{\text{K-R}}$ is also used in equation (7). Given the great complexity in establishing time delays between solar wind quantities and the PCN index, a cross correlation analysis provides only an approximation to the precise time delay, but the uncertainty does not mask the correlations that we are studying. Time delays between AL and $E_{\text{K-R}}$ should, in principle, also be taken into account. However, the time for convection from Qaanaaq to AE stations is expected to be on the order of 10 min, whereas, for our cases, the time scale for AL index to decrease and recover is on the order of hours Gao et al. (submitted manuscript, 2012). Thus, we do not consider additional delays in correlating $E_{\text{K-R}}$ and AL.

[15] The linear model, equation (12), makes a strong assumption about the dependence of PCN on $E_{\text{K-R}}$ and AL_{U}, namely that the dependence is linear in each of the
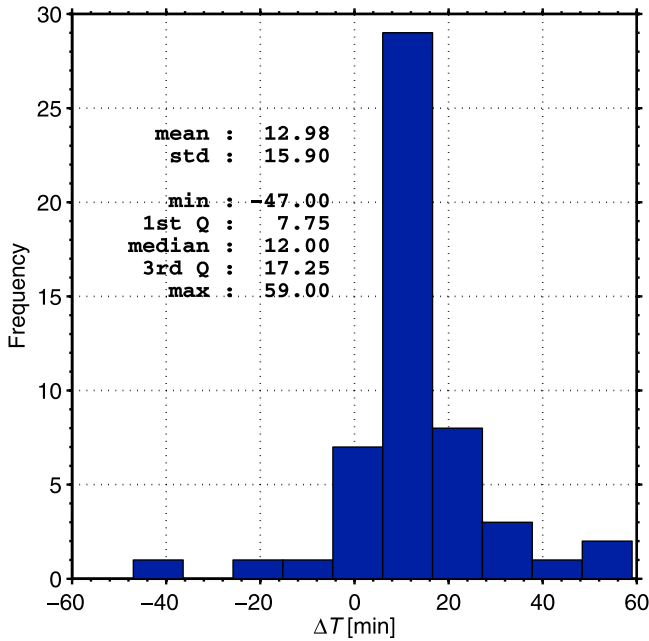
Figure 1. Histogram of additional time shifts of the solar wind data for events used in Gao et al. (submitted manuscript, 2012).

predictors. If this assumption holds, even roughly, then the linear regression model is useful and convenient, because (i) it provides a simple description of the data, (ii) it summarizes the relative contribution of each predictor with a single coefficient, and (iii) it provides a simple method for predicting new observations.

[16] Nevertheless, when fitting a linear regression model, we generally do not assert that the model is correct. Rather we believe that it will be a good first order approximation to the true solution, and that we can uncover the important predictors and their roles using the approximation. It is, however, legitimate to question the validity of the linear assumption. One way to test the validity is to employ a more general, nonlinear model to perform the analysis and compare the results with those obtained from the linear analysis.

3.1. Additive Model

[17] An important feature of the linear regression model (e.g., equation (12)) is the additive nature among the predictors. Once we have fitted the linear model we can examine the predictor effects separately in the absence of interactions. There are many ways to generalize a linear regression model. Of these, the additive model [*Stone*, 1985; *Hastie and Tibshirani*, 1990] is particularly appealing as it retains this important feature of the linear model: it is additive in the predictor effects. Therefore, for our test of nonlinearity, we have selected the additive model, which is

$$PCN = \alpha + f_1(E_{\text{K-R}}) + f_2(\text{AL}_\text{U}) + \varepsilon_\text{A}, \quad (13)$$

where α is intercept, $f_1(E_{\text{K-R}})$ and $f_2(\text{AL}_\text{U})$ are arbitrary univariate (depending on only one variable) smooth

functions of $E_{\text{K-R}}$ and AL_U respectively and ε_A is Gaussian noise. If $f_1(E_{\text{K-R}})$ and α are redefined as

$$f_1^*(E_{\text{K-R}}) = f_1(E_{\text{K-R}}) + c, \text{and } \alpha^* = \alpha - c, \quad (14)$$

where c is an constant, equation (13) remains unchanged. Thus, to uniquely determine the values of $f_1(E_{\text{K-R}})$ and $f_2(\text{AL}_\text{U})$, two constraints are imposed on equation (13) [*Stone*, 1985; *Hastie and Tibshirani*, 1986, 1990], i.e.

$$\text{E}(f_1(E_{\text{K-R}})) = 0, \text{and } \text{E}(f_2(\text{AL}_\text{U})) = 0, \quad (15)$$

where $\text{E}(X)$ stands for the expectation of X.

3.2. Backfitting Algorithm

[18] The additive model is fitted by the "backfitting algorithm" [*Hastie and Tibshirani*, 1990]. Notice that the conditional expectations of equation (13) require that

$$f_1(E_{\text{K-R}}) = \text{E}(f_1(E_{\text{K-R}})|E_{\text{K-R}}) = \text{E}(\text{PCN} - \alpha - f_2(\text{AL}_\text{U})|E_{\text{K-R}}), \quad (16)$$

$$f_2(\text{AL}_\text{U}) = \text{E}(f_2(\text{AL}_\text{U})|\text{AL}_\text{U}) = \text{E}(\text{PCN} - \alpha - f_1(E_{\text{K-R}})|\text{AL}_\text{U}), \quad (17)$$

where $\text{E}(Y|X = x)$ represents the expectation of Y conditional on $X = x$. Define $\text{PCN} - \alpha - f_2(\text{AL}_\text{U})$ and $\text{PCN} - \alpha - f_1(E_{\text{K-R}})$ as the partial residuals of $E_{\text{K-R}}$ and AL_U respectively, i.e.

$$pr(E_{\text{K-R}}) = \text{PCN} - \alpha - f_2(\text{AL}_\text{U}), \quad (18)$$

$$pr(\text{AL}_\text{U}) = \text{PCN} - \alpha - f_1(E_{\text{K-R}}). \quad (19)$$

Starting with an initial guess, $f_2^{(0)}(\text{AL}_\text{U})$ which usually takes a linear form, the additive model can be fitted by iteratively smoothing the partial residuals, i.e.

$$f_1^{(t+1)}(E_{\text{K-R}}) = S\left(\text{PCN} - \alpha - f_2^{(t)}(\text{AL}_\text{U})\right), \quad (20)$$

$$f_2^{(t+1)}(\text{AL}_\text{U}) = S\left(\text{PCN} - \alpha - f_1^{(t+1)}(E_{\text{K-R}})\right), \quad (21)$$

where t records the iteration step, i.e., $t = 0, 1, \ldots$, and S is a smoothing operator discussed in section 3.3. Iterations are terminated when $f_1^{(t+1)}(E_{\text{K-R}}) \approx f_1^{(t)}(E_{\text{K-R}})$ and $f_2^{(t+1)}(\text{AL}_\text{U}) \approx f_2^{(t)}(\text{AL}_\text{U})$. *Hastie and Tibshirani* [1990] provide further details of the backfitting algorithm, e.g., derivation, convergence, rate of convergence, uniqueness of solutions.

3.3. Locally Weighted Scatterplot Smoothing

[19] An effective approach to extracting a nonlinear representation of scattered data that relates to familiar methods such as least squares regression is referred to as the LOESS (LOcally wEighted Scatterplot Smoothing) method [*Cleveland*, 1979]. The method provides a rigorous approach to obtain a fit to scattered data, or "smoothing" it, by joining the centroids of local straight line fits to portions of the data. In smoothing data values, for each point x_0, k nearest points, denoted by $N(x_0)$, are identified. The distance of the furthest point in the set $N(x_0)$ from x_0 is computed as

$$\Delta(x_0) = \max_{x_i \in N(x_0)} |x_0 - x_i|. \quad (22)$$
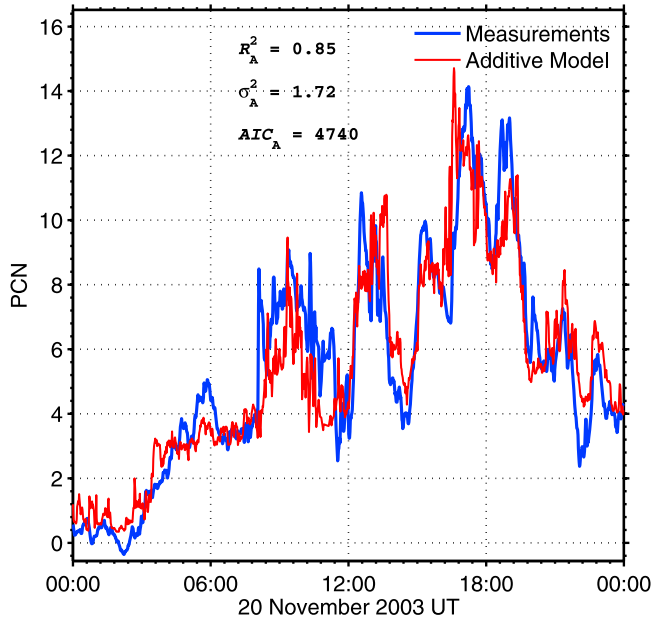
Figure 2. Comparison between the measured PCN index (blue line) and the predicted PCN index from an additive model (red line) based on solar wind parameters for the storm of 20 November 2003. R_A^2, σ_A^2 are computed to estimate goodness of fit and AIC_A is used to estimate the model optimality.

Weights w_i are assigned to each point in $N(x_0)$, using the tri-cube weight function $W(| x_0 - x_i |/\Delta(x_0))$, where

$$W(u) = \left[(1 - u^3)^3 \right]_+ \qquad (23)$$

Here $[x]_+ = x$, if $x > 0$, otherwise $[x]_+ = 0$. The predicted value at x_0 is fitted from the (local) weighted least squares fit confined to $N(x_0)$ using the weights computed above. Thus, our model becomes

$$PCN = \alpha + lo(E_{K\text{-}R}, k_1) + lo(AL_U, k_2) + \varepsilon_A, \qquad (24)$$

where lo stands for LOESS. Here k_1 and k_2, the numbers of nearest neighbors, determine the smoothness of the additive bases, $lo(E_{K\text{-}R}, k_1)$ and $lo(AL_U, k_2)$, respectively and ε_A is assumed to be Gaussian noise. Diverse choices of k_1 and k_2 are discussed in *Hastie and Tibshirani* [1990] in detail and will not be pursued here. A popular choice is to fix $k_1 = k_2 = 0.5n$ [*Hastie and Tibshirani*, 1990] to guarantee enough smoothness, where n is the number of observations. This strategy is adopted in this study and k_1, k_2 will be omitted in later discussions. The computational details are summarized in the following backfitting algorithm.

[20] *Algorithm 1* (The backfitting algorithm). Initialize $\alpha = \beta_0, f_1^{(0)}(E_{K\text{-}R}) = \beta_1 zs(E_{K\text{-}R})$, and $f_2^{(0)}(AL_U) = \beta_2 zs(AL_U)$ from the results of linear regression (equation (12)). For $t = 0, 1$, ..., :

[21] 1. Compute $f_1^{(t+1)}(E_{K\text{-}R}) = $ LOESS(PCN $- \alpha - f_2^{(t)}(AL_U), 0.5n$);

[22] 2. Compute $f_2^{(t+1)}(AL_U) = $ LOESS(PCN $- \alpha - f_1^{(t+1)}$ $(E_{K\text{-}R}), 0.5n$);

[23] 3. If $\|f_1^{(t+1)}(E_{K\text{-}R}) - f_1^{(t)}(E_{K\text{-}R})\| < \delta$ and $\|f_2^{(t+1)}(AL_U) - f_2^{(t)}(AL_U)\| < \delta$, stop; otherwise, repeat 1 and 2.

Here $\|x\|$ stands for the Euclidean norm of a vector x, and δ is a pre-defined small number.

[24] In steps 1 and 2, the notation LOESS(x, k) is adopted in order to emphasize that smoothing of x is achieved by using the LOESS technique with k nearest neighbors.

[25] Ideally, $lo(E_{K\text{-}R})$ and $lo(AL_U)$ in equation (24) are obtained from $lo(E_{K\text{-}R}) = f_1^{(\infty)}(E_{K\text{-}R})$ and $lo(AL_U) = f_2^{(\infty)}(AL_U)$. For finite iterations, if the stopping criterion is satisfied after T steps, then $lo(E_{K\text{-}R}) \approx f_1^{(T)}(E_{K\text{-}R})$ and $lo(AL_U) \approx f_2^{(T)}(AL_U)$.

3.4. Inference

[26] An event on 20 November 2003, shown in Figure 2, can help us better understand the approach. In Figure 2, the blue line is the measured PCN and the red line is the predicted PCN based on the nonlinear additive model. The consistency between measurements and predictions is apparent.

[27] In order to quantify the performances of the linear model and the additive model, three statistics, coefficient of determination (R^2), error variance (σ^2) and Akaike's information criterion (AIC) [*Akaike*, 1974], are computed to estimate the goodness of fit and model optimality. R^2, varying between 0 and 1, represents the variation in the response variable that is explained by the model [*Myers*, 2000; Gao et al., submitted manuscript, 2012]. σ^2 is calculated from the variance of the residuals [*Myers*, 2000]. Both R^2 and σ^2 quantify the goodness of fit of a model. AIC, different from R^2 and σ^2, not only rewards the goodness of fit, but also penalizes the model complexity. Given a set of possible models for the data, the optimal model is the one with the minimum AIC value. A detailed discussion on the definitions and properties of the above statistics is given in Appendix A.
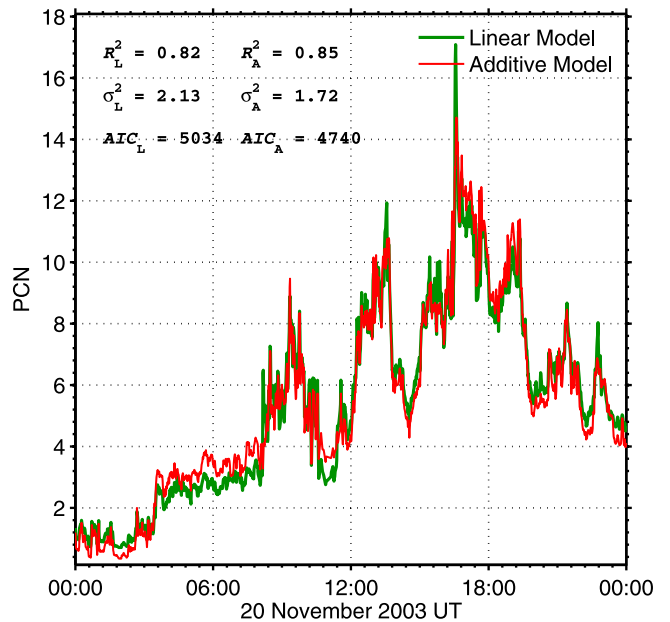

Figure 3. Comparison between linear model (green line) and additive model (red line) for the case of 20 November 2003. The change of R^2, error variance and AIC can be used to assess the performance of different models.
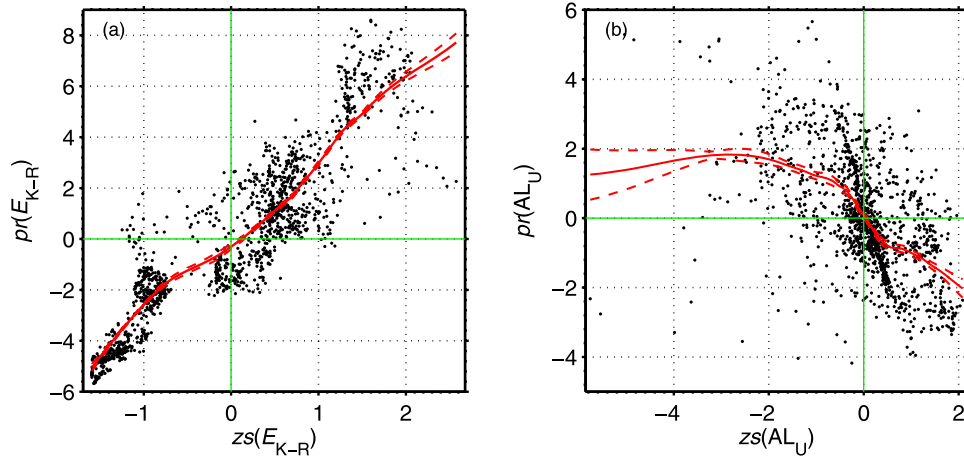
Figure 4. Relation of partial residuals $pr(E_{K\text{-}R})$, $pr(AL_U)$ and linear bases $zs(E_{K\text{-}R})$, $zs(AL_U)$ for the case on 20 November 2003. The scatters are between the partial residuals and their corresponding z-scores, i.e., $pr(E_{K\text{-}R})$ versus $zs(E_{K\text{-}R})$, and $pr(AL_U)$ versus $zs(AL_U)$. The red solid lines are the functional relation (a) between $lo(E_{K\text{-}R})$ and $zs(E_{K\text{-}R})$ and (b) between $lo(AL_U)$ and $zs(AL_U)$. The red dashed lines give the corresponding 95% pointwise confidence intervals. The green lines label $zs(E_{K\text{-}R}) = 0$ and $pr(E_{K\text{-}R}) = 0$ (Figure 4, left) and $zs(AL_U) = 0$ and $pr(AL_U) = 0$ (Figure 4, right).

[28] For the event on 20 November 2003, the values of PCN predicted by the fitted values from the additive model and from the linear model, i.e.

$$PCN = 5.45_{(0.04)} + 2.94_{(0.04)}\,zs(E_{K\text{-}R}) - 0.91_{(0.04)}\,zs(AL_U), \quad (25)$$

are shown in Figure 3. The numbers in the parentheses in the equation above are the standard deviations of the corresponding regression coefficients. The additive model slightly outperforms the linear model with increased R^2 (from 0.82 to 0.85), decreased error variance (from 2.13 to 1.72) and reduced AIC (from 5034 to 4740). The fitted values from the two models are extremely similar. Figure 4 compares the estimated partial residuals of the additive model with the linear bases. The black dots indicate the scatters between the partial residuals and the linear bases, i.e., $pr(E_{K\text{-}R})$ versus $zs(E_{K\text{-}R})$ and $pr(AL_U)$ versus $zs(AL_U)$. The red solid lines, calculated by

smoothing the scatters, are $lo(E_{K\text{-}R})$ and $lo(AL_U)$ as functions of $zs(E_{K\text{-}R})$ and of $zs(AL_U)$, respectively. The red dashed lines are the corresponding estimated 95% pointwise confidence intervals. The green lines partition the region with $zs(E_{K\text{-}R}) = 0$ and $pr(E_{K\text{-}R}) = 0$ (left) and $zs(AL_U) = 0$ and $pr(AL_U) = 0$ (right). It is clear that $lo(E_{K\text{-}R})$ roughly bears a linear relationship with $zs(E_{K\text{-}R})$, but some nonlinearity between $lo(AL_U)$ and $zs(AL_U)$ develops for this event. Nevertheless, the part with significant deviation from linearity of AL_U lies in the strong geomagnetic activity limit where there are few observations. Thus, if a linear relationship between $lo(AL_U)$ and $zs(AL_U)$ is assumed, no significant error is introduced, which is confirmed by the close correspondence between the fitted values from the linear model and those from the additive model (Figure 3).

[29] We have also tested the performance of $E_{K\text{-}L}$ as a regression basis in the additive model. Since no saturation
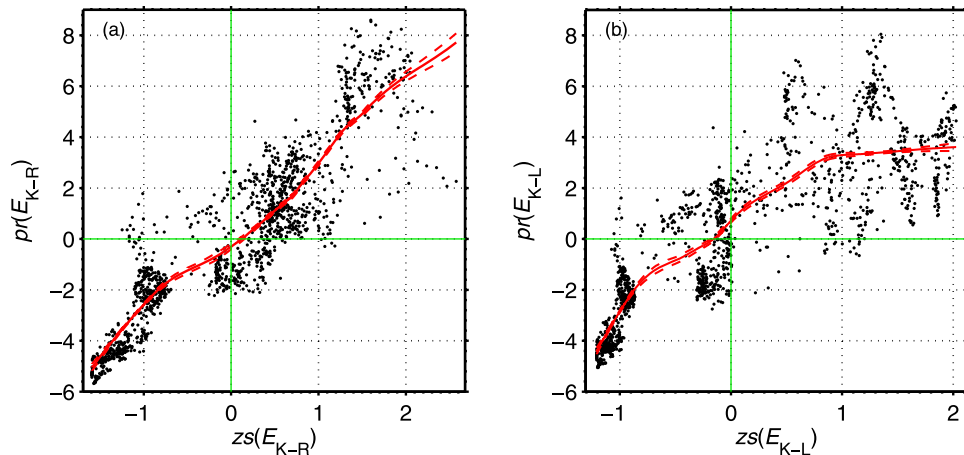

Figure 5. (a) Partial residual of $E_{K\text{-}R}$ versus its linear basis. (b) Partial residual of $E_{K\text{-}L}$ versus its linear basis on 20 November 2003. The format is the same as Figure 4.
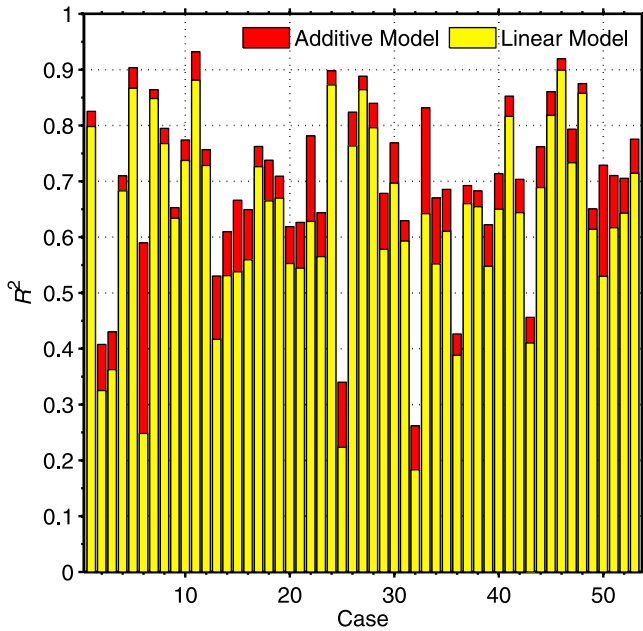
Figure 6. R^2 for the linear model and the additive model. The yellow bars indicate the R^2 values for the linear model (R_L^2) and the red bars plotted beneath the yellow bars (but extending to higher values of R^2) give the changes of R^2 by switching from linear model to additive model ($R_A^2 - R_L^2$).

Figure 7. Akaike's information criterion (AIC) for the linear model and the additive model. The red bars are the AIC's for additive analysis (AIC_A) for all the cases. The yellow bars (this time plotted below the red bars but extending above them) on top of the red bars indicate the increases of AIC from additive model to linear model ($AIC_L - AIC_A$).

mechanism is included in $E_{K\text{-}L}$, prominent nonlinearity between $lo(E_{K\text{-}L})$ and $zs(E_{K\text{-}L})$ is expected under strong solar wind driving. For the case on 20 November 2003, this is confirmed in Figure 5. Figure 5a displays the additive basis, $lo(E_{K\text{-}R})$, as an approximately linear function of the linear basis, $zs(E_{K\text{-}R})$, of $E_{K\text{-}R}$. Nevertheless, in Figure 5b, $lo(E_{K\text{-}L})$ levels off at large values of $zs(E_{K\text{-}L})$. The nonlinear relationship between $lo(E_{K\text{-}L})$ and $zs(E_{K\text{-}L})$ is clear.

[30] The same comparisons between the linear model and the additive model, using $E_{K\text{-}R}$ and AL_U as predictors, have been applied to all the cases. The results are summarized in Figures 6 and 7, which show the change of R^2 and change of AIC from the linear model to the additive model. For all the cases, the additive model systematically outperforms the linear model with increased R^2 and decreased AIC. Nevertheless, the improvements are relatively small.

[31] A more direct approach is to compare the fitted values of the linear model with those of the additive model by calculating their correlation coefficients whose distribution is shown in Figure 8. The correlation coefficients concentrate near 1 with only one exception on 18 February 1999. The nonlinearity between the additive bases and linear bases for this case is clear as shown in Figure 9. It also corresponds to the largest increase of R^2 from the linear model to the additive model in Figure 6. For this case, the prediction from the linear model fails with $R^2 = 0.25$ as is shown in Figure 10. Moreover, significant difference between PCS and PCN are found between 0600UT and 1200UT (not shown here). This case will be discussed in detail by the authors in a later report. In a future study, it will also be of interest to systematically investigate the consistency and contrast between the fitted values from the additive model
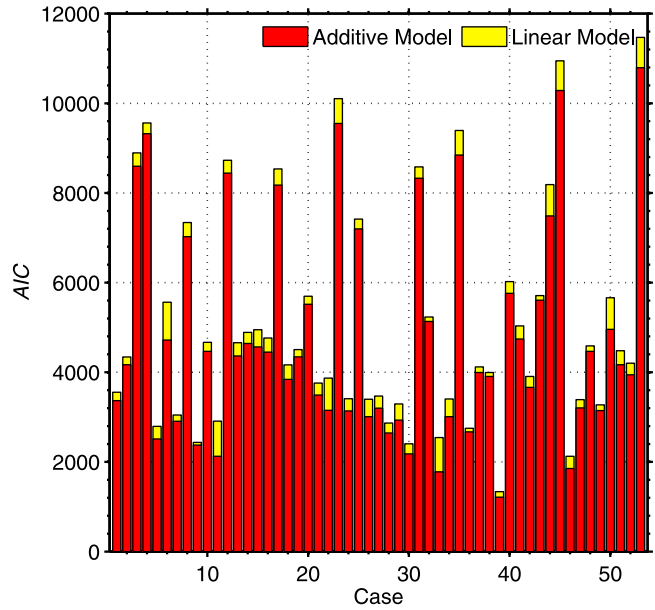
and those from the linear model for various levels of geomagnetic activity.

[32] Furthermore, it is of great importance to compare the relative contributions to PCN from two predictors in the additive model and compare the result with that obtained from the linear model. Unlike the linear model for which the
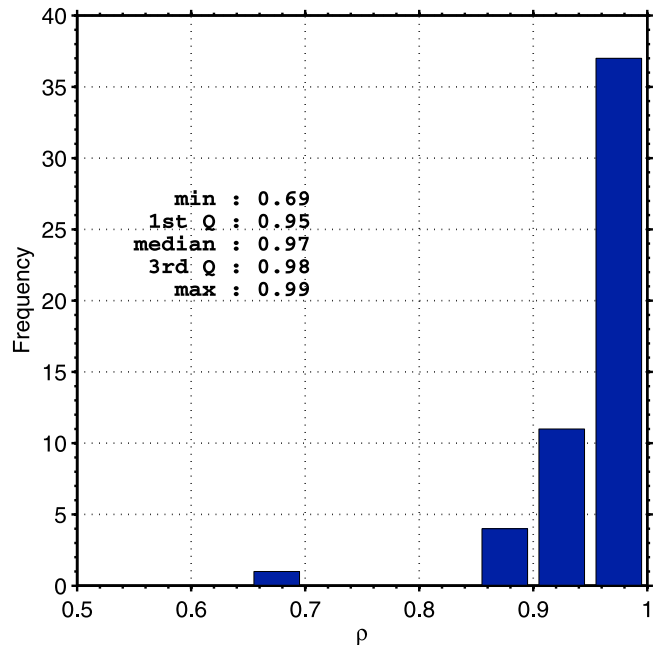

Figure 8. Histogram of correlation coefficients of fitted values to the linear model and the additive model.
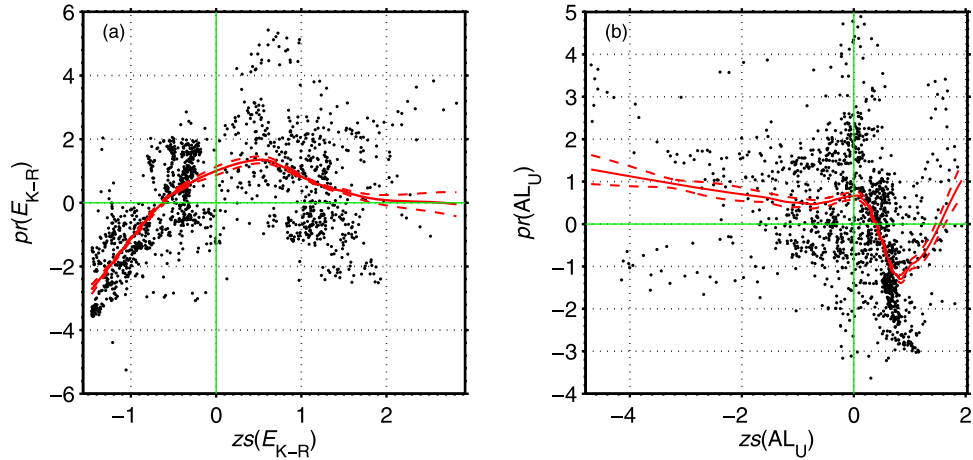
Figure 9. As for Figure 4 for the event on 18 February 1999.

contribution of each predictor is summarized in a regression coefficient, the contribution of a predictor in an additive model, $E_{K\text{-}R}$ say, has to be calculated from its additive basis, i.e., $lo(E_{K\text{-}R})$. The standard deviation of lo $(E_{K\text{-}R})$ and that of $lo(AL_U)$ summarize the contributions to PCN from $E_{K\text{-}R}$ and AL_U respectively, and thus, can be used to compare their relative importance in controlling PCN. Figure 11 shows a scatterplot of the standard deviations of $lo(E_{K\text{-}R})$, denoted as $|\sigma_{lo(E_{K\text{-}R})}|$, and $lo(AL_U)$, similarly written as $|\sigma_{lo(AL_U)}|$, for those cases with $R_A^2 \geq 0.5$. The points are both colored and scaled according to their R_A^2 values. An orthogonal regression between $|\sigma_{lo(AL_U)}|$ and $|\sigma_{lo(E_{K\text{-}R})}|$ forced to pass through origin is

added as the blue line. The regression coefficient, 0.47, indicates that the contribution of $E_{K\text{-}R}$ to PCN is roughly twice as important as AL_U in an additive model. This is consistent with the result of Gao et al. (submitted manuscript, 2012) based on the linear assumption between the PCN index and $E_{K\text{-}R}$, AL_U.

[33] If the potential nonlinearity between AL and $E_{K\text{-}R}$ is taken into account, an additive model can be used to derive the unloading AL, denoted as $AL_{U,A}$ here, i.e.

$$AL_{U,A} = AL - AL_{D,A}, \qquad (26)$$

where

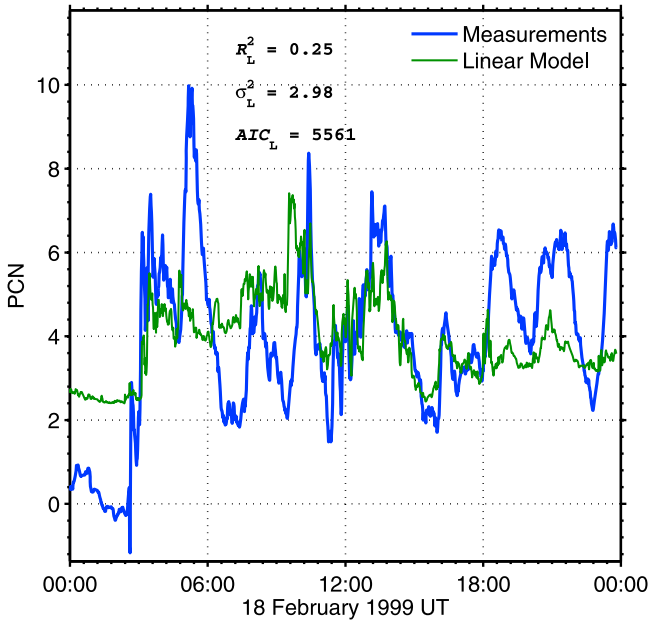$$AL_{D,A} = \alpha_0 + lo(E_{K\text{-}R}, 0.5n). \qquad (27)$$

Figure 10. Comparison between measured PCN (blue line) and predicted PCN based on linear model (green line) on 18 February 1999. This is the only case during which the additive model gives inconsistent results with those obtained from the linear model.
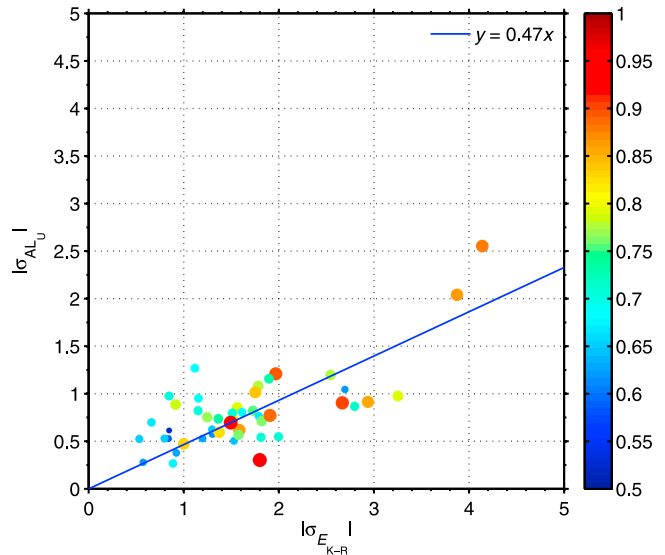

Figure 11. Scatterplot of standard deviations of $lo(AL_U)$ versus that of $lo(E_{K\text{-}R})$ for those cases with $R_A^2 \geq 0.5$. The points are both colored and scaled according to the corresponding R_A^2. An orthogonal regression between $|\sigma_{lo(AL_U)}|$ and $|\sigma_{lo(E_{K\text{-}R})}|$ in blue line was forced to pass through origin.

Accordingly, the additive model, equation (24), is updated to

$$\text{PCN} = \alpha' + lo(E_{\text{K-R}}, 0.5n) + lo(\text{AL}_{\text{U,A}}, 0.5n) + \varepsilon'_{\text{A}}. \tag{28}$$

We have found that the results obtained by using equation (28) are quite similar to those obtained by using equation (24). Besides, it is more convenient to examine the differences between the additive model and the linear model, if the same variable, AL_{U}, is used in the two models. For example, in Figure 4b, we have compared the additive basis, $lo(\text{AL}_{\text{U}})$, directly with the linear basis, $zs(\text{AL}_{\text{U}})$. However, if, instead, $\text{AL}_{\text{U,A}}$ is used, then we are only able to compare $lo(\text{AL}_{\text{U,A}})$ with $zs(\text{AL}_{\text{U,A}})$, which is not used in the linear model. Therefore, in this paper, we have reported the results obtained by using equation (24).

4. Discussion and Conclusions

[34] In this report, we studied the response of polar cap dynamics as characterized by the PCN index to solar wind parameters and geomagnetic activity under strong solar wind driving by extending the linear regression analysis of Gao et al. (submitted manuscript, 2012) between PCN and $E_{\text{K-R}}$, AL_{U} to a more general, nonlinear model, i.e., an additive model (equation (24)). Here, $E_{\text{K-R}}$ is used as a representative of the electric field imposed on the ionosphere by magnetopause reconnection, modified to account for saturation. We have compared the results with those obtained from the linear model (equation (12)) by using the same cases as that used in Gao et al. (submitted manuscript, 2012). We found that although, in general, the additive model outperforms the linear model with increased R^2 and decreased AIC, the improvements obtained by switching from a linear model to an additive model are small. Thus, the validity of the linear assumption is confirmed. The fitted values from the two models are extremely similar to each other, with the distribution of the correlation coefficient between the linear fits and the additive fits concentrating near 1 with one exception, an event on 18 February 1999. This is an anomalous case that will be discussed fully in a later report. With one exception, the results from the two models are quite similar. They both tell us that $E_{\text{K-R}}$ is approximately twice as important as AL_{U} in controlling PCN, which is the same result reported by Gao et al. (submitted manuscript, 2012). Although the additive model of PCN as a response to $E_{\text{K-R}}$ and AL_{U} is more flexible in the sense that it does not require that PCN varies linearly with the independent quantities, the linear model already provides a very good approximation. Furthermore, the linear model gives a simpler description of the data by summarizing the contribution of each predictor in a regression coefficient and is easier to be extended to more advanced analysis, e.g., robust regression. The usage of a linear model in this problem is highly encouraged.

Appendix A

[35] In this appendix, we provide the definitions and properties of the statistics used in this study, i.e., coefficient of determination (R^2), error variance (σ^2) and Akaike's information criterion (AIC).

[36] For ease of discussion, we define $\mathbf{y}$ as the vector of observations and $\hat{\mathbf{y}}_+$ as the vector of additive fits. It is important to notice that to fit an additive model is equivalent to generating a mapping from $\mathbf{y}$ to $\hat{\mathbf{y}}_+$, i.e.

$$\hat{\mathbf{y}}_+ = \mathbf{R}\mathbf{y}, \tag{A1}$$

where $\mathbf{R}$ is the mapping matrix. Then, R^2, σ^2 and AIC can be computed from $\mathbf{y}$, $\hat{\mathbf{y}}_+$ and $\mathbf{R}$.

[37] For an additive model, the coefficient of determination, i.e., R_{A}^2, is defined as [Hastie and Tibshirani, 1990; Myers, 2000]

$$R_{\text{A}}^2 = 1 - D(\mathbf{y}; \hat{\mathbf{y}}_+)/D(\mathbf{y}; \bar{y}\mathbf{1}). \tag{A2}$$

In the above equation, $D(\mathbf{y}; \hat{\mathbf{y}}_+)$ is the deviance, calculated as

$$D(\mathbf{y}; \hat{\mathbf{y}}_+) = \|\mathbf{y} - \hat{\mathbf{y}}_+\|^2, \tag{A3}$$

where $\mathbf{y} - \hat{\mathbf{y}}_+$ is the model residual vector, $\|\mathbf{x}\|$ indicates the Euclidean norm of vector $\mathbf{x}$. $D(\mathbf{y}; \bar{y}\mathbf{1})$, the null deviance, is defined as

$$D(\mathbf{y}; \bar{y}\mathbf{1}) = \| \mathbf{y} - \bar{y}\mathbf{1}\|^2, \tag{A4}$$

where $\bar{y}$ is the sample mean and $\mathbf{1} = (1, 1, \ldots, 1)^{\text{T}}$. R_{A}^2, varying between 0 and 1, can be interpreted as the fraction of variations explained by the model [Myers, 2000; Gao et al., submitted manuscript, 2012]. The error variance for an additive model is calculated as

$$\sigma_{\text{A}}^2 = D(\mathbf{y}; \hat{\mathbf{y}}_+)/df_{\text{err}}. \tag{A5}$$

Here df_{err}, the error degree of freedom, is computed from [Hastie and Tibshirani, 1990]

$$df_{\text{err}} = n - \text{tr}(2\mathbf{R} - \mathbf{R}\mathbf{R}^T), \tag{A6}$$

where n is the number of observations, $\mathbf{R}$ is the mapping matrix in equation (29) and tr($\mathbf{A}$) stands for the trace of matrix $\mathbf{A}$. R_{L}^2 and σ_{L}^2 for the linear model can be similarly defined by replacing $\hat{\mathbf{y}}_+$ with the least square fits, $\hat{\mathbf{y}}_{\text{LS}}$, of a linear model, i.e.

$$R_{\text{L}}^2 = 1 - D(\mathbf{y}; \hat{\mathbf{y}}_{\text{LS}})/D(\mathbf{y}; \bar{y}\mathbf{1}), \tag{A7}$$

and df_{err} with $n - p$, i.e.

$$\sigma_{\text{L}}^2 = D(\mathbf{y}; \hat{\mathbf{y}}_{\text{LS}})/(n - p), \tag{A8}$$

where p is the number of parameters, e.g., $p = 3$ for equation (13) [Myers, 2000]. As to Akaike's information criterion (AIC), in general, it is defined as [Akaike, 1974]

$$AIC = -2\ln L + 2p, \tag{A9}$$

where L is the maximized value of the likelihood function for the estimated model and p is still the number of parameters in a model. Given a set of candidate models for the data, the preferred model is the one with the minimum AIC value, since AIC not only rewards goodness of fit, but also includes a penalty that is an increasing function of the number of estimated parameters. In practice, a convenient

form arises from writing $\ln(L)$ as [*Burnham and Anderson*, 2002]

$$\ln(L) = C - (n/2)\ln(D(\mathbf{y};\hat{\mathbf{y}})/n), \qquad (A10)$$

where $\mathbf{y}$ is the vector of observations, $\hat{\mathbf{y}}$ is the vector of fitted values, and C is a constant independent of the model used. Thus, *AIC* becomes

$$AIC_L = n\ln(D(\mathbf{y};\hat{\mathbf{y}}_{LS})/n) + 2p - 2C \qquad (A11)$$

for a linear model, or

$$AIC_A = n\ln\big(D(\mathbf{y};\hat{\mathbf{y}}_+)/n\big) + 2\,\mathrm{tr}(\mathbf{R}) - 2C \qquad (A12)$$

for an additive model. In the above equation, $\mathrm{tr}(\mathbf{R})$, an estimator of p, is the effective number of parameters of an additive model [*Hastie and Tibshirani*, 1990].

[38] It is important to notice that a reduced form of *AIC*, denoted as AIC_R, is used in Gao et al. (submitted manuscript, 2012),

$$AIC_R = \ln\sigma_m^2 + (n+2p)/n, \qquad (A13)$$

where $\sigma_m^2 = SS_{Res}/n$. Since SS_{Res} in Gao et al. (submitted manuscript, 2012) is the same as the $D(\mathbf{y};\hat{\mathbf{y}}_{LS})$ here, AIC_R is related to *AIC* through

$$AIC_R = (AIC + n - 2C)/n. \qquad (A14)$$

Consequently, the *AIC* values obtained from this study are consistent with those reported by Gao et al. (submitted manuscript, 2012), although they look different.

References

Akaike, H. (1974), A new look at the statistical model identification, *IEEE Trans. Autom. Control*, *19*(6), 716–723, doi:10.1109/TAC.1974.1100705.

Akasofu, S. I. (1979), What is a magnetospheric substorm?, in *Dynamics of Magnetosphere*, edited by S. I. Akasofu, pp. 447–460, D. Reidel, Dordrecht, Netherlands, doi:10.1007/978-94-009-9519-2_23.

Bargatze, L. F., D. N. Baker, E. W. Hones Jr., and R. L. McPherron (1985), Magnetospheric impulse response for many levels of geomagnetic activity, *J. Geophys. Res.*, *90*, 6387–6394, doi:10.1029/JA090iA07p06387.

Borovsky, J. E., B. Lavraud, and M. M. Kuznetsova (2009), Polar cap potential saturation, dayside reconnection, and changes to the magnetosphere, *J. Geophys. Res.*, *114*(A3), A03224, doi:10.1029/2009JA014058.

Burnham, K., and D. Anderson (2002), *Model Selection and Multimodel Inference: A Practical Information-Theoretic Approach*, Springer, New York.

Chun, F. K., D. J. Knipp, M. G. McHarg, G. Lu, B. A. Emery, S. Vennerstrøm, and O. A. Troshichev (1999), Polar cap index as a proxy for hemispheric Joule heating, *Geophys. Res. Lett.*, *26*, 1101–1104, doi:10.1029/1999GL900196.

Chun, F. K., D. J. Knipp, M. G. McHarg, J. R. Lacey, G. Lu, and B. A. Emery (2002), Joule heating patterns as a function of polar cap index, *J. Geophys. Res.*, *107*(A7), 1119, doi:10.1029/2001JA000246.

Cleveland, W. S. (1979), Robust locally weighted regression and smoothing scatterplots, *J. Am. Stat. Assoc.*, *74*(368), 829–836, doi:10.2307/2286407.

Fiori, R. A. D., A. V. Koustov, D. Boteler, and R. A. Makarevich (2009), PCN magnetic index and average convection velocity in the polar cap inferred from SuperDARN radar measurements, *J. Geophys. Res.*, *114*, A07225, doi:10.1029/2008JA013964.

Gao, Y., M. G. Kivelson, R. J. Walker, and J. M. Weygand (2012), Long-term variation of driven and unloading effects on polar cap dynamics, *J. Geophys. Res.*, *117*(A2), A02203, doi:10.1029/2011JA017149.

Hastie, T. J., and R. J. Tibshirani (1986), Generalized additive models, *Stat. Sci.*, *1*(3), 297–310, doi:10.1214/ss/1177013604.

Hastie, T. J., and R. J. Tibshirani (1990), *Generalized Additive Models*, CRC Press, Boca Raton, Fla.

Hill, T. W., A. J. Dessler, and R. A. Wolf (1976), Mercury and Mars: The role of ionospheric conductivity in the acceleration of magnetospheric particles, *Geophys. Res. Lett.*, *3*(8), 429–432, doi:10.1029/GL003i008p00429.

Kan, J. R., and L. C. Lee (1979), Energy coupling function and solar wind-magnetosphere dynamo, *Geophys. Res. Lett.*, *6*, 577–580, doi:10.1029/GL006i007p00577.

Kivelson, M. G., and A. J. Ridley (2008), Saturation of the polar cap potential: Inference from Alfvén wing arguments, *J. Geophys. Res.*, *113*, A05214, doi:10.1029/2007JA012302.

Liou, K., J. F. Carbary, P. T. Newell, C.-I. Meng, and O. Rasmussen (2003), Correlation of auroral power with the polar cap index, *J. Geophys. Res.*, *108*(A3), 1108, doi:10.1029/2002JA009556.

McComas, D. J., S. J. Bame, P. Barker, W. C. Feldman, J. L. Phillips, P. Riley, and J. W. Griffee (1998), Solar Wind Electron Proton Alpha Monitor (SWEPAM) for the Advanced Composition Explorer, *Space Sci. Rev.*, *86*(1–4), 563–612, doi:10.1023/A:1005040232597.

McPherron, R. L., and D. N. Baker (1993), Factors influencing the intensity of magnetospheric substorms, *J. Atmos. Terr. Phys.*, *55*(8), 1091–1122, doi:10.1016/0021-9169(93)90040-6.

Myers, R. H. (2000), *Classical and Modern Regression With Applications*, 2nd ed., Duxbury, Boston.

Nagatsuma, T. (2002), Saturation of polar cap potential by intense solar wind electric fields, *Geophys. Res. Lett.*, *29*(10), 1422, doi:10.1029/2001GL014202.

Ridley, A. J., and E. A. Kihn (2004), Polar cap index comparisons with AMIE cross polar cap potential, electric field, and polar cap area, *Geophys. Res. Lett.*, *31*, L07801, doi:10.1029/2003GL019113.

Russell, C. T., G. Lu, and J. G. Luhmann (2000), Lessons from the ring current injection during the September 24, 25, 1998 storm, *Geophys. Res. Lett.*, *27*(9), 1371–1374, doi:10.1029/1999GL003718.

Shepherd, S. G., R. A. Greenwald, and J. M. Ruohoniemi (2002), Cross polar cap potentials measured with Super Dual Auroral Radar Network during quasi-steady solar wind and interplanetary magnetic field conditions, *J. Geophys. Res.*, *107*(A7), 1094, doi:10.1029/2001JA000152.

Siscoe, G. L., G. M. Erickson, B. U. Ö. Sonnerup, N. C. Maynard, J. A. Schoendorf, K. D. Siebert, D. R. Weimer, W. W. White, and G. R. Wilson (2002), Hill model of transpolar potential saturation: Comparisons with MHD simulations, *J. Geophys. Res.*, *107*(A6), 1075, doi:10.1029/2001JA000109.

Siscoe, G. L., J. Raeder, and A. J. Ridley (2004), Transpolar potential saturation models compared, *J. Geophys. Res.*, *109*(A9), A09203, doi:10.1029/2003JA010318.

Smith, C. W., J. L'Heureux, N. F. Ness, M. H. Acuña, L. F. Burlaga, and J. Scheifele (1998), The ACE Magnetic Fields Experiment, *Space Sci. Rev.*, *86*(1–4), 613–632, doi:10.1023/A:1005092216668.

Stauning, P. (2011), Comment on "The PC index: review of methods", by McCreadie and Menvielle (2010), *Ann. Geophys.*, *29*(6), 1137–1146, doi:10.5194/angeo-29-1137-2011.

Stone, C. J. (1985), Additive regression and other nonparametric models, *Ann. Stat.*, *13*(2), 689–705, doi:10.1214/aos/1176349548.

Troshichev, O. A., and R. Y. Lukianova (2002), Relation of PC index to the solar wind parameters and substorm activity in time of magnetic storms, *J. Atmos. Terr. Phys.*, *64*, 585–591, doi:10.1016/S1364-6826(02)00016-0.

Troshichev, O. A., V. G. Andrezen, S. Vennerstrom, and E. Friis-Christensen (1988), Magnetic activity in the polar cap—A new index, *Planet. Space Sci.*, *36*, 1095–1102, doi:10.1016/0032-0633(88)90063-3.

Troshichev, O. A., H. Hayakawa, A. Matsuoka, T. Mukai, and K. Tsuruda (1996), Cross polar cap diameter and voltage as a function of PC index and interplanetary quantities, *J. Geophys. Res.*, *101*, 13,429–13,435, doi:10.1029/95JA03672.

Troshichev, O. A., R. Y. Lukianova, V. O. Papitashvili, F. J. Rich, and O. Rasmussen (2000), Polar cap index (PC) as a proxy for ionospheric electric field in the near-pole region, *Geophys. Res. Lett.*, *27*, 3809–3812, doi:10.1029/2000GL003756.

Weimer, D. R., D. M. Ober, N. C. Maynard, M. R. Collier, D. J. McComas, N. F. Ness, C. W. Smith, and J. Watermann (2003), Predicting interplanetary magnetic field (IMF) propagation delay times using the minimum variance technique, *J. Geophys. Res.*, *108*(A1), 1026, doi:10.1029/2002JA009405.